nature cell biology

Sequential functioning of the ECT-2 RhoGEF, RHO-1 and CDC-42 establishes cell polarity in *Caenorhabditis elegans* embryos

Fumio Motegi[1] and Asako Sugimoto[1,2]

During development, the establishment of cell polarity is important for cells to undergo asymmetric cell divisions that give rise to diverse cell types. In *C. elegans* embryos, cues from the centrosome trigger the cortical flow of an actomyosin network, leading to the formation of anterior–posterior polarity[1]. However, its precise mechanism is poorly understood. Here, we show that small GTPases have sequential and crucial functions in this process. ECT-2, a potential guanine nucleotide-exchange factor (GEF)[2] for RHO-1, was uniformly distributed at the cortex before polarization, but was excluded from the posterior cortex by the polarity cue from the centrosomes. This local exclusion of ECT-2 led to an asymmetric RHO-1 distribution, which generated a cortical flow of the actomyosin that translocated PAR proteins[3] and CDC-42 (refs 4, 5) to the anterior cortex. Polarized CDC-42 was, in turn, involved in maintaining the established anterior-cortical domains. Our results suggest that a local change in the function of ECT-2 and RHO-1 links the centrosomal polarity cue with the polarization of the cell cortex.

For a cell to become polarized, a polarity cue triggers reorganization of the cell cortex, which then establishes cytoplasmic asymmetry. *C. elegans* embryos become polarized along their anterior–posterior axis shortly after fertilization[3,6]. The polarity cue seems to be linked to the sperm-donated centrosome[7,8], which defines the posterior pole of the embryo. When the centrosome repositions near the cortex, the polarity cue triggers asymmetric cortical contraction — cortical smoothing begins at the posterior pole and spreads anteriorly, whereas the anterior cortex continues to ruffle. Polarity of cortical ruffling precisely corresponds to the asymmetric distribution of PAR proteins. A widely conserved PAR protein complex, which consists of PAR-3, PAR-6 and atypical protein kinase C (PKC-3), becomes enriched at the anterior cortex and inhibits the association of PAR-2 with the cortex, thus allowing PAR-2 to localize at the complementary posterior cortex[3,9]. After the pronuclear migration, the polarized PAR proteins mediate asymmetric positioning of mitotic spindles and asymmetric partitioning of cell-fate determinants.

The actomyosin cytoskeleton has crucial roles in the polarization process[1,10–13] and a model has been proposed in which the contractile actomyosin network initiates an anteriorly directed cortical flow to transport the PAR-3–PAR-6–PKC-3 complex[1]. Two members of the Rho subfamily of small GTPases, RHO-1 and CDC-42, are potent regulators of the actomyosin cytoskeleton in a variety of contexts[14]. CDC-42 is required for asymmetric PAR distribution in the early *C. elegans* embryo[4,5], but the mode of action of CDC-42 has been unclear. Although RHO-1 and its potential GEF, ECT-2 (also known as LET-21, ref. 2) are involved in cytokinesis[15–17], whether they are involved in the establishment of anterior–posterior polarity is not known. We therefore examined the processes that establish anterior–posterior polarity in embryos that were depleted of CDC-42, RHO-1 or ECT-2 by RNA-mediated interference (RNAi).

RNAi against *cdc-42*, *rho-1* or *ect-2* genes resulted in 100% embryonic lethality by 24–30 h after RNAi treatment and the amounts of the corresponding proteins were estimated to be reduced to <9%, <6% and <6% of wild-type animals, respectively (see Supplementary Information, Fig. S1a, b). RHO-1 and ECT-2, in addition to CDC-42 (ref. 4, 5), are required for asymmetric spindle positioning during anaphase (Fig. 1). In wild-type one-cell embryos, the posterior pole of the mitotic spindle moves posteriorly during anaphase. This movement was significantly decreased in the *ect-2 (RNAi)* and *rho-1 (RNAi)* embryos, and was also compromised in the *cdc-42 (RNAi)* embryos as previously reported[4,5], which implies that these three embryos were defective in establishing anterior–posterior polarity in one-cell embryos. Although cortical ruffling and posterior cortical smoothing were detected in *cdc-42 (RNAi)* embryos (100%; 20 of 20), both events were not observed in *ect-2 (RNAi)* (100%; 17 of 17) and *rho-1 (RNAi)* (95%; 18 of 19) embryos, indicating that ECT-2 and RHO-1 may have roles that are distinct from that of CDC-42 in the establishment of anterior–posterior polarity. These results prompted us to examine the roles of these genes in PAR protein distribution and actomyosin reorganization during the establishment of anterior–posterior polarity.

[1]Laboratory for Developmental Genomics, RIKEN Center for Developmental Biology, 2-2-3 Minatojima-minamimachi, Chuo-ku, Kobe, 650-0047, Japan.
[2]Correspondence should be addressed to A.S. (e-mail: sugimoto@cdb.riken.jp)

Received 12 May 2006; accepted 16 June 2006; published online 20 August 2006; DOI: 10.1038/ncb1459

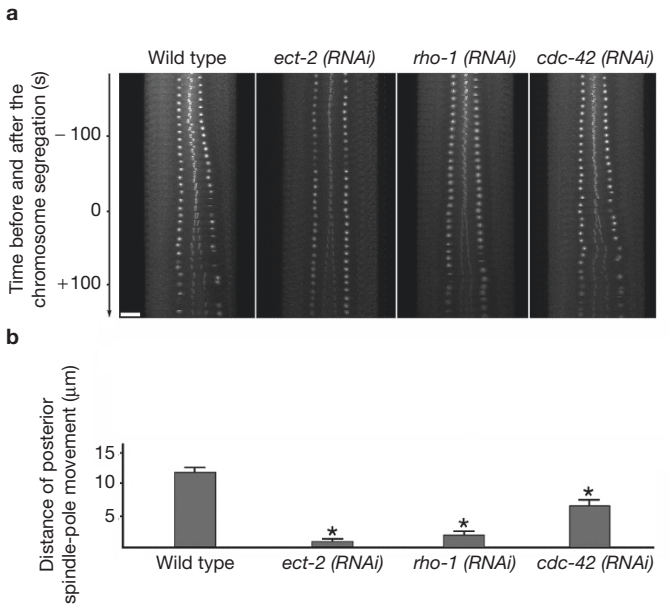

Figure 1 CDC-42, RHO-1 and ECT-2 are required for asymmetric spindle positioning in the one-cell embryo. (**a**) Kymographs from time-lapse images of GFP–PLK-1 at the medial focal plane. In this and subsequent figures, embryos are oriented with the anterior pole to the left. GFP–PLK-1 was detected at centrosomes, chromosomes and the spindle midzone. Times are with respect to the onset of chromosome segregation (s). The scale bar represents 10 μm. (**b**) Comparisons of the distance of posterior spindle pole movement from metaphase (–170 s) to telophase (+140 s). Asterisks indicate a statistically significant difference between wild-type embryos and the RNAi-treated embryos (Student's *t*-test, $P < 0.05$). The data represent the mean ± s.d. ($n = 6$ for wild-type, *ect-2* and *rho-1*; $n = 8$ for *cdc-42*).

The cortical dynamics of the actomyosin cytoskeleton and the anterior PAR proteins were characterized during the polarization process by monitoring the GFP-tagged filamentous actin-binding domain of *Drosophila melanogaster* moesin (GFP–moe)[15] and PAR-6 (GFP–PAR-6)[9], respectively (Fig. 2a, b). In the fertilized embryo, both proteins were uniformly distributed in the cell cortex; GFP–moe was detected as a meshwork and GFP–PAR-6 was detected as particles. Time-lapse recordings of these cortical proteins enabled us to distinguish between two distinct phases of establishment of anterior–posterior polarity. In the first phase (before pronuclear migration), GFP–PAR-6 particles and GFP–moe signals moved toward the anterior cortex. Consequently, GFP–PAR-6 particles were virtually excluded from the posterior half of the embryo and GFP–moe signals were enriched in the anterior cortex. In the second phase (during pronuclear migration), the punctate GFP–PAR-6 signals became smoother, suggesting rearrangement of the GFP–PAR-6 organization at the anterior cortex (Fig. 2a, b). Concomitantly, the fluorescence intensities of GFP–moe at the anterior cortex increased (Fig. 2a, b, d). Hereafter, we refer to the first phase of polarization by anteriorly directed cortical flows as phase I, and to the second phase, during which the reorganization of the anterior cortical domain seems to occur, as phase II.

To understand the function of CDC-42, RHO-1 and ECT-2 in the polarization process, GFP–PAR-6 and GFP–moe were monitored at the cell cortex in live embryos, which were depleted of these genes by RNAi (Fig. 2c, d). In phase I, although GFP–PAR-6 particles accumulated in the anterior cortical domain in wild-type embryos, in embryos depleted of ECT-2 or RHO-1, only a small amount of GFP–PAR-6 was associated with the cortex and this cortically located GFP–PAR-6 did not move toward the anterior cortex (Fig. 2c and see Supplementary Information, Fig. S2a), indicating that ECT-2 and RHO-1 are required for the initial polarization of PAR protein in phase I. In contrast, the cortical GFP–PAR-6 particles in *cdc-42 (RNAi)* embryos were virtually normal in their number and accumulation in the anterior cortex in phase I, but the localized PAR-6 disappeared in phase II. Thus, consistent with previous reports[4], CDC-42 seems to be dispensable for the asymmetric distribution of PAR-6 in phase I, but it is essential in phase II for the maintenance of the anteriorly localized PAR-6.

The dynamics of cortical actin filaments, as visualized by GFP–moe, were consistent with those for GFP–PAR-6 (Fig. 2d and see Supplementary Information, Fig. S2b). In wild-type embryos, GFP–moe was enriched in the anterior domain in phase I. The *ect-2 (RNAi)* and *rho-1 (RNAi)* embryos did not localize GFP–moe to the cortex in phase I, indicating that ECT-2 and RHO-1 are required to generate the cortical actomyosin network in phase I. In contrast, *cdc-42 (RNAi)* embryos showed normal enrichment of GFP–moe in the anterior domain in phase I, but the accumulated GFP–moe disappeared in phase II. These results indicate that ECT-2, RHO-1 and CDC-42 have different roles during the formation of cortical asymmetry: ECT-2 and RHO-1 are required for the formation and contraction of cortical actomyosin and for asymmetric PAR distribution during phase I; and CDC-42 is essential in phase II for the maintenance of the anterior cortical domain generated in phase I.

Whereas *rho-1 (RNAi)* embryos failed to form a cortical actin network in phase I, strong GFP–moe signals were observed in a large cortical domain during phase II (Fig. 2d); however, the GFP–moe signals were not necessarily enriched on the anterior side of embryos, unlike the wild-type (100%, 8 of 8; Fig. 2d, e). Thus, phase II embryos are capable of forming a cortical actin network in the absence of RHO-1 activity, although such a cortical actin network is no longer properly polarized. Codepletion of RHO-1 and CDC-42 completely suppressed the formation of the high GFP–moe region (100%, 7 of 7; Fig. 2d), suggesting that CDC-42 is involved in the formation of a cortical actin network independently of RHO-1 in phase II. The aberrant formation of the cortical actin network in phase II was not observed in *ect-2 (RNAi)* embryos, implying that ECT-2 may affect not only RHO-1 activity, but also CDC-42 activity, either directly or indirectly.

We next examined the localization of ECT-2, RHO-1 and CDC-42 tagged with GFP that were expressed in the germline and early embryos under the control of the germline-specific *pie-1* promoter. Immunoblotting with GFP antibodies recognized each GFP-fusion protein as a band of the correct estimated molecular mass and each band substantially decreased after RNAi against the corresponding gene (see Supplementary Information, Fig. S1a, b). The amount of GFP–RHO-1 was 4% that of the endogenous RHO-1 protein in the transgenic animals (see Supplementary Information, Methods, and data not shown); thus the GFP signals that were detected were unlikely to be an artifact that occurred because of overexpression. Furthermore, GFP–RHO-1 distribution in transgenic lines matched the distribution as detected by immunostaining (see below and Supplementary Information, Fig. S1c). GFP-fusion proteins are thus likely to reflect the behaviour of the endogenous protein. (As we could not obtain antibodies against ECT-2 and CDC-42, we were unable to confirm the endogenous expression and localization of these proteins.)

GFP–ECT-2 was monitored at the medial focal plane in wild-type embryos (Fig. 3a, b and see Supplementary Information, Movie 1).

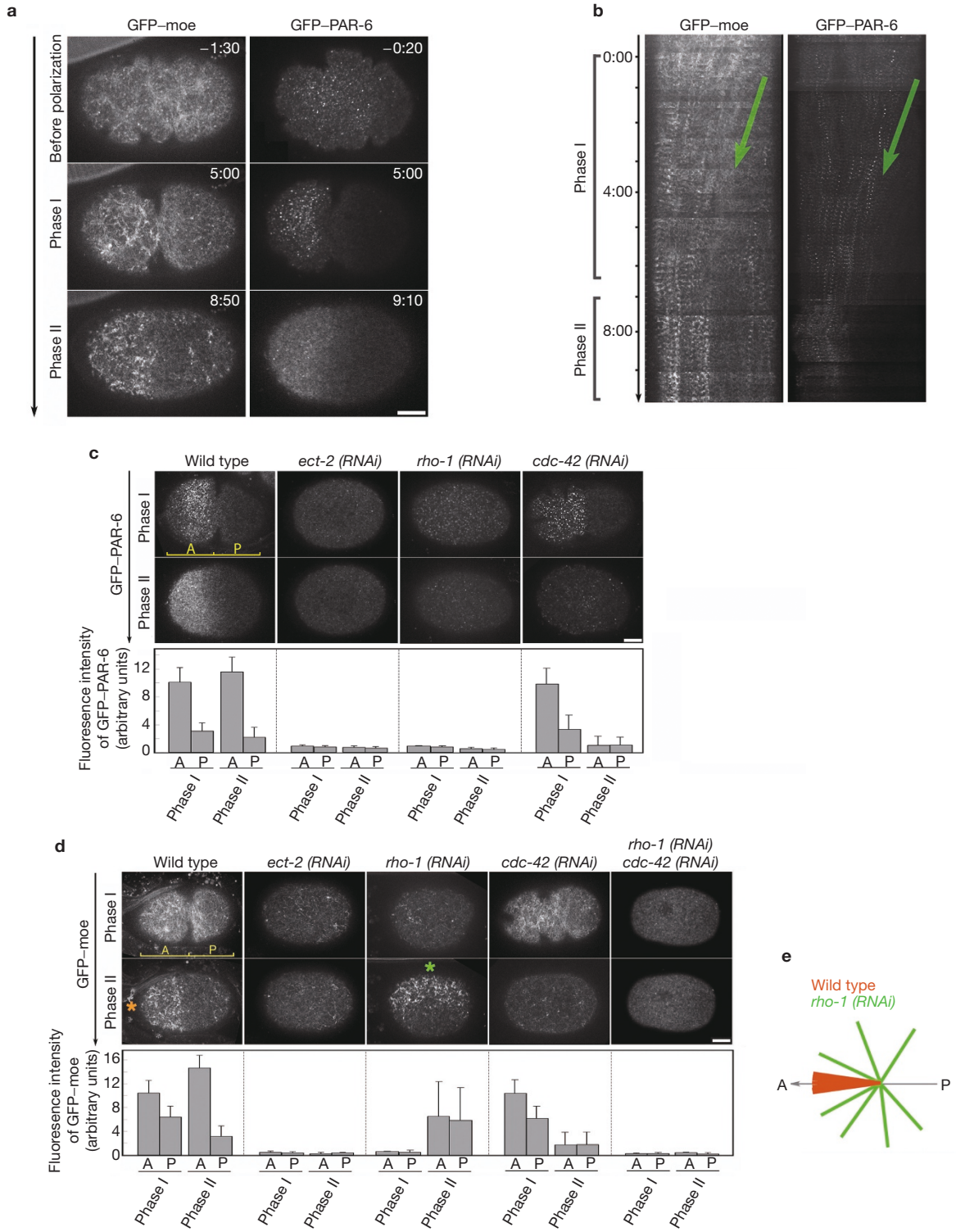

Figure 2 RHO-1 and CDC-42 have distinct roles in anterior–posterior polarization. (**a**, **b**) Two distinct steps occur during the establishment of anterior–posterior polarity: initial polarization (phase I) and reorganization of the anterior cortex (phase II). Time-lapse images (**a**) and kymographs (**b**) of GFP–moe and GFP–PAR-6 at the cortex, before and during polarization, are shown. Green arrows indicate a selected trajectory of the GFP signals in phase I. Times are with respect to the onset of posterior cortical smoothing (min:s). (**c**, **d**) RHO-1 and its potential GEF, ECT-2, mediate the initial polarization, and CDC-42 functions to maintain the polarized cortex. Images of GFP–PAR-6 (**c**) and GFP–moe (**d**) at the cortex in phase I and II from the time-lapse recordings of a single representative embryo are shown. The graphs indicate the quantification of the fluorescence intensity (mean ± s.d. of 7 embryos) within the anterior and posterior half of the cortex (see Methods). The orange asterisk in **d** indicates anteriorly accumulated GFP–moe in the wild-type embryo and the green asterisk indicates the abnormally oriented large region of GFP–moe in the *rho-1 (RNAi)* embryo. (**e**) Orientation of GFP–moe accumulation in wild-type (orange) and *rho-1* RNAi (green) embryos after the pronuclear migration. Results from 7 embryos are shown in each case. A, anterior; P, posterior. The scale bars represent 10 μm in **a**, **c** and **d**.

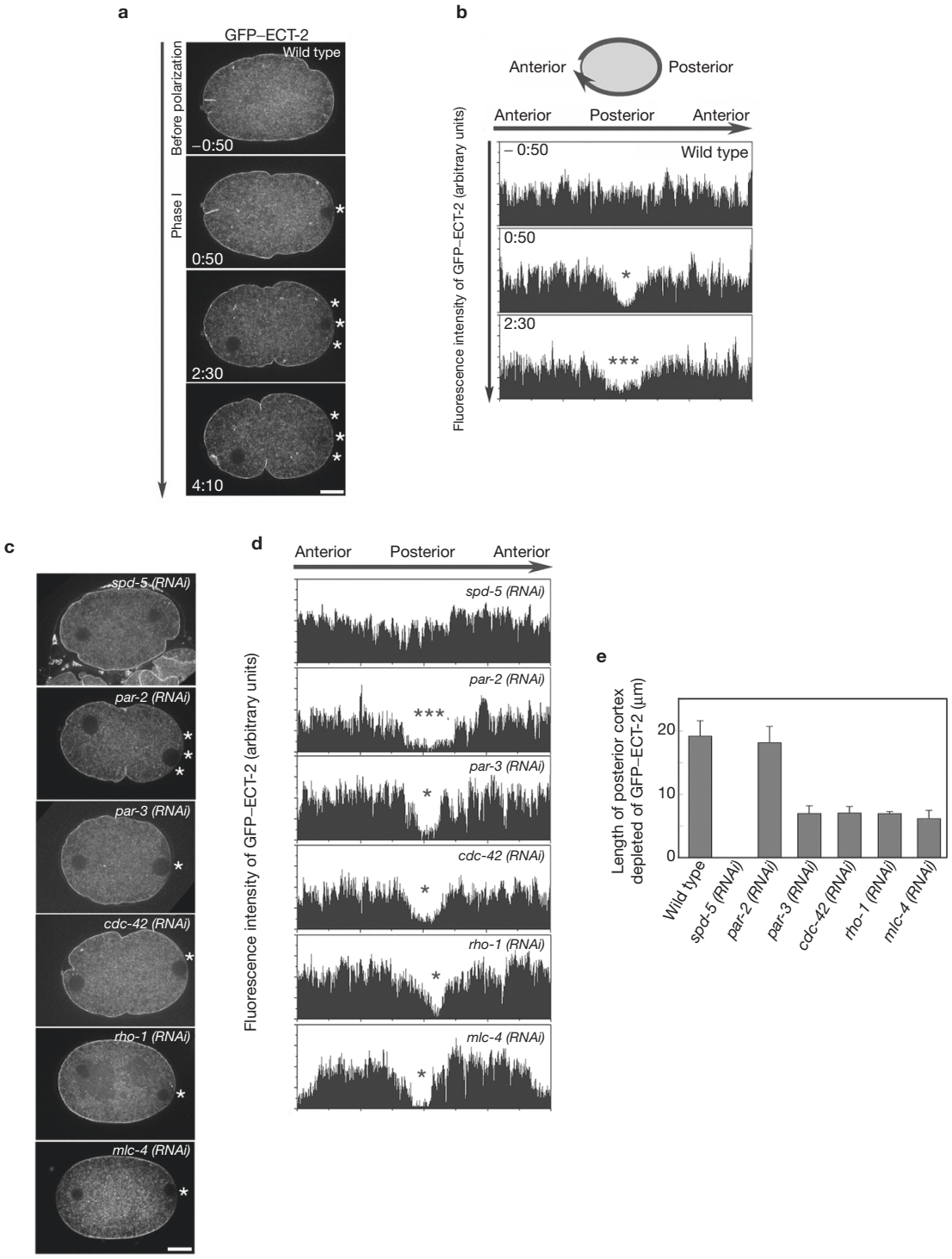

Figure 3 The centrosome mediates exclusion of cortical ECT-2. (**a**) Time-lapse images of GFP–ECT-2 at the medial focal plane during polarization. Asterisks indicate the cortex near the sperm pronuclei where cortical GFP–ECT-2 is excluded. Times are with respect to the onset of posterior cortical smoothing (min:s). (**b**) Line-scan analysis of fluorescence intensities of cortical GFP–ECT-2 during polarization. In the schematic, a curved line from anterior pole to anterior pole marks the cortical region from which the line scan was made. This curve was linearized to generate the line scan. Asterisks indicate the extent of the cortical region that was depleted of GFP–ECT-2. (**c**, **d**) Initial exclusion of GFP–ECT-2 from the posterior cortex requires SPD-5 but not Rho GTPases, PAR proteins or the actomyosin cytoskeleton. Images of GFP–ECT-2 at the medial focal plane in phase I at the time when the GFP-ECT-2-depeleted cortical region was most expanded are shown in **c**. Line-scan analysis of the fluorescence intensities of cortical GFP–ECT-2 from the images in **c** are shown in **d**. Asterisks indicate the cortical region that was depleted of GFP–ECT-2. (**e**) Comparison of the maximum length of cortical regions depleted of GFP–ECT-2 during phase I. The data represent the mean ± s.d. (n = 7 for wild type, *spd-5* and *par-2*; n = 8 for *par-3*, *cdc-42*, *rho-1* and *mlc-4*). The scale bars represent 10 μm in **a** and **c**.

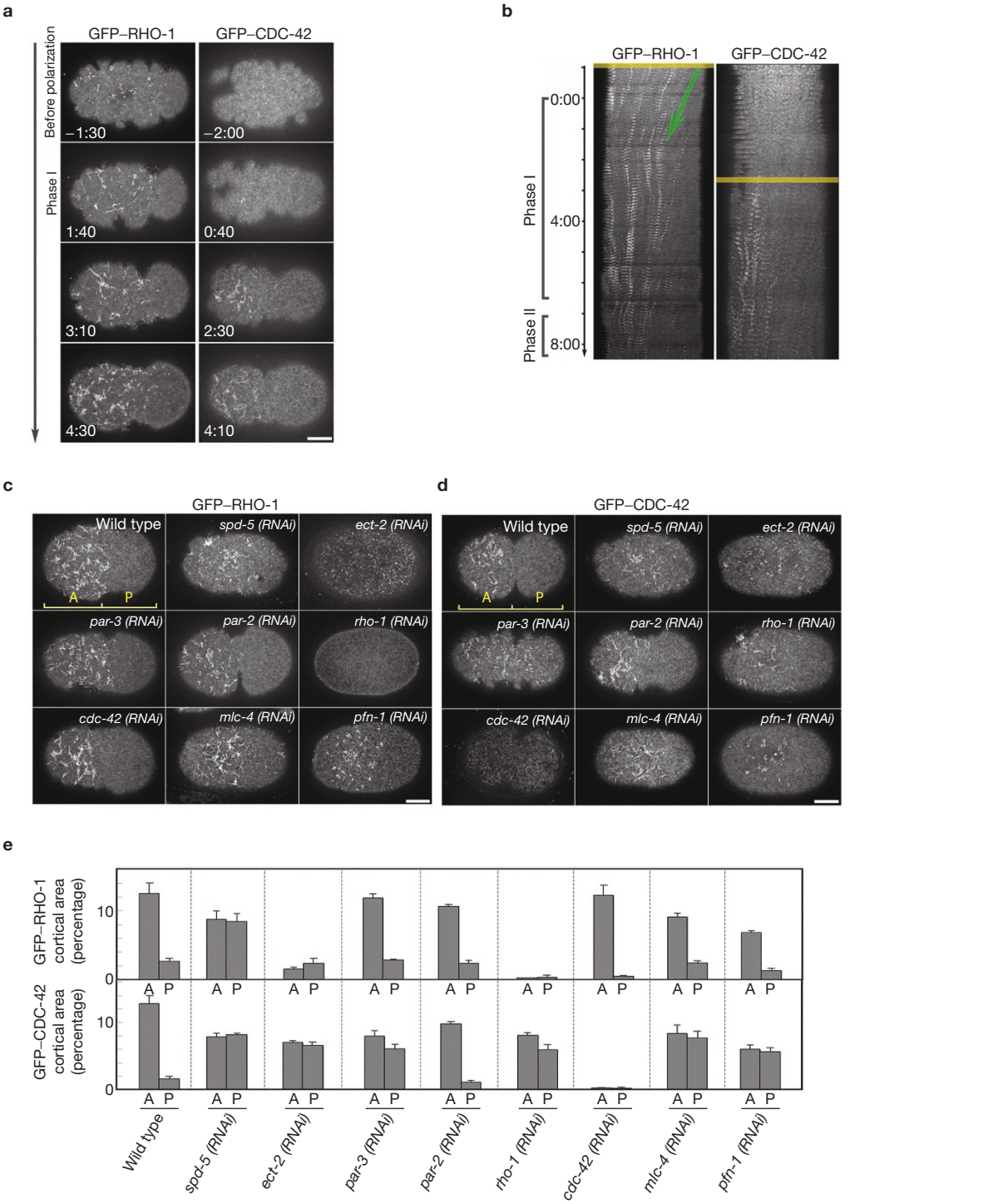

Figure 4 Asymmetric distribution of cortical foci of RHO-1 and CDC-42. (**a**, **b**) GFP–RHO-1 flows away from the posterior pole and GFP–CDC-42 appears at the anterior cortex during the cortical flow. Time-lapse images (**a**) and kymographs (**b**) of GFP–RHO-1 and GFP–CDC-42 at the cortex of wild-type embryos are shown. The green arrow tracks a selected trajectory and the yellow line indicates the timing of the appearance of GFP–RHO-1 and GFP–CDC-42 foci at the cortex. Times are with respect to the onset of posterior cortical smoothing (min:s). (**c**, **d**) Distribution of cortical GFP–RHO-1 and GFP–CDC-42 foci in wild-type embryos and RNAi embryos defective in the establishment of anterior–posterior polarity. Images were collected at the transition from phase I to phase II. (**e**) Quantification of the asymmetry of cortical foci of GFP–RHO-1 and GFP–CDC-42. The percentage of the area covered by the cortical foci within the anterior and posterior half of the embryos at the onset of phase II are shown. The data represent the mean ± s.d. of (n = 7 for wild type; n = 6 for all others). The scale bars represent 10 μm in **a**, **c** and **d**.

Before polarization, GFP–ECT-2 was distributed uniformly throughout the cortex. After the onset of posterior cortical smoothing (when polarization was initiated), the GFP–ECT-2 signal was locally decreased at the cortex nearest the sperm pronuclei, where the centrosomes are located. As posterior cortical smoothing progressed in phase I, the cortical region that was depleted of GFP–ECT-2

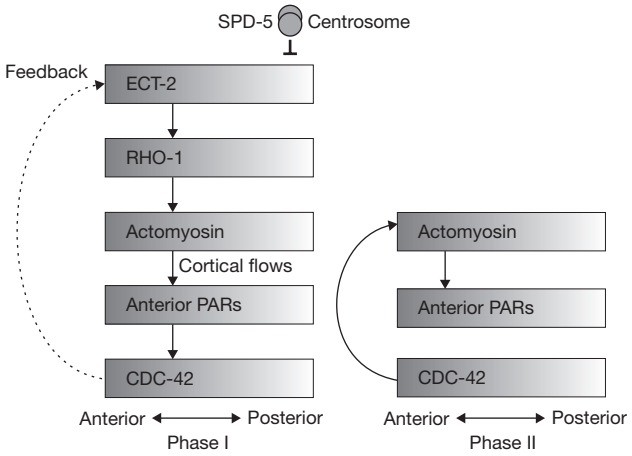

Figure 5 A schematic representation of a model for the establishment of anterior–posterior polarity in the *C. elegans* one-cell embryo. The centrosomal polarity cue mediated through SPD-5 function acts to exclude ECT-2 from the posterior cortex, which causes a local depletion of RHO-1. This asymmetric distribution of RHO-1 generates a cortical flow of the actomyosin network, probably through a gradient of cortical tensions. The cortical actomyosin flow translocates PAR proteins and CDC-42 to the anterior cortex. Concomitantly, CDC-42 seems to promote the enrichment of ECT-2 (dotted line). After the initial polarization, CDC-42 mediates a reorganization of the actomyosin to maintain the anterior cortical domain of PAR proteins.

expanded anteriorly and as the pronuclei migrated, GFP–ECT-2 signals were gradually recovered at the posterior cortical region (see Supplementary Information, Movie 1). This exclusion of GFP–ECT-2 was not caused by an artifact of association of the sperm pronuclei with the cortex as the plasma membrane marker GFP–$PH^{PLC1\delta1}$ (ref. 18) did not exhibit local exclusion during this stage (see Supplementary Information, Fig. S3). When the centrosomal protein SPD-5 (which is required to make a functional centrosome[19]) was depleted, cortical exclusion of GFP–ECT-2 was not observed (Fig. 3c, d). On the other hand, in embryos depleted of PAR-3, RHO-1, CDC-42, MLC-4 (a myosin light chain protein; Fig. 3c, d) or PFN-1 (profilin, which is involved in actin polymerization; data not shown), initial exclusion of GFP–ECT-2 from the most posterior cortex was not affected, but the subsequent expansion of the GFP–ECT-2-depleted domain was compromised in these embryos (Fig. 3e). In *mlc-4 (RNAi)* embryos, GFP–ECT-2 was also depleted from a region of anterior cortex. In *par-2 (RNAi)* embryos, both initiation and expansion of GFP–ECT-2 exclusion were unaffected. Thus, PAR proteins, RHO-1, CDC-42 and the actomyosin cytoskeleton are dispensable for the initial exclusion of ECT-2 from the posterior cortex, whereas SPD-5 is an essential component of this process.

In wild-type embryos, GFP–RHO-1 is also dynamic — unlike the uniform cortical localization of GFP–ECT-2, it was found as small foci and short filaments throughout the cortex before polarization (Fig. 4a,b and see Supplementary Information, Movie 2). During phase I, these GFP–RHO-1 foci moved away from the posterior cortex and coalesced into larger clumps at the anterior cortex, resulting in an enrichment of the GFP–RHO-1 foci at the anterior cortex. New GFP–RHO-1 foci also seemed to form at the anterior cortex during this stage. The cortical foci located throughout the cortex before polarization, and the anteriorly accumulated foci at mitotic prophase, are consistent with immunofluorescence microscopy analysis of wild-type embryos with anti-RHO-1 (see Supplementary Information, Fig. S1c). Anterior enrichment of GFP–RHO-1 foci during phase I was observed in *par-3 (RNAi)*, *par-2 (RNAi) cdc-42 (RNAi) mlc-4 (RNAi)* and *pfn-1 (RNAi)* embryos (Fig. 4c, e). In contrast, cortical GFP–RHO-1 foci were symmetrically distributed in *spd-5 (RNAi)* embryos (Fig. 4c, e), indicating that asymmetric distribution of cortical RHO-1 requires SPD-5 function. In *ect-2 (RNAi)* embryos, GFP–RHO-1 signals were not detected as cortical foci, but were observed as small cytoplasmic particles with a weak fluorescence intensity that was uniformly distributed (Fig. 4c, e). Thus, the generation of RHO-1 cortical foci seems to require ECT-2 function, and it is plausible that activation of RHO-1 is involved in its own proper localization, as previously reported for other cellular contexts (for examples see refs 15, 20, 21). These results place ECT-2 and SPD-5 upstream of RHO-1 among the components that function in the formation of the asymmetric actomyosin network and in PAR-6 distribution. These results suggest that the local exclusion of ECT-2 from the cortex leads to delocalization of RHO-1 at the posterior cortex, generating an asymmetric gradient of cortical RHO-1.

The spatiotemporal distribution of CDC-42 was distinct from that of RHO-1. Before and during the early stage of phase I, structured GFP–CDC-42 signals were not detected at the cell cortex (Fig. 4a, b and see Supplementary Information, Movie 3). Small foci and short filaments of GFP–CDC-42 predominantly appeared at the anterior cortex during the late stages of phase I — later than those of GFP–RHO-1 (Fig. 4a,b). Anterior enrichment of cortical foci of GFP–CDC-42 during phase I was not observed in *spd-5 (RNAi), ect-2 (RNAi), par-3 (RNAi) rho-1 (RNAi), mlc-4 (RNAi)* and *pfn-1 (RNAi)* embryos (Fig. 4d, e), or in *par-3 (RNAi)* or *par-2 (RNAi)* embryos (data not shown), whereas it occurred in *par-2 (RNAi)* embryos. These data suggest that the asymmetric gradient of RHO-1, in addition to the subsequent actomyosin flow and asymmetric PAR-3 distribution, is required for the asymmetric distribution of cortical CDC-42 foci.

We noted that in *rho-1 (RNAi)*, *mlc-4 (RNAi)*, *par-3 (RNAi)* and *cdc-42 (RNAi)* embryos, the GFP–ECT-2-depleted cortical region did not expand in phase I, although it did expand in wild-type embryos (Fig. 3e). These molecules that affect the expansion of the ECT-2-depleted domain are all enriched at the anterior cortex during phase I. Thus, it is reasonable to speculate that these anterior cortical proteins are involved in the promotion of the anterior expansion of the ECT-2-depleted domain. On the other hand, our results also place ECT-2 upstream of RHO-1, actomyosin and PAR-3, which are in turn required for asymmetric distribution of CDC-42. A simple interpretation for the relationship between these anterior proteins during phase I is that anteriorly enriched CDC-42 modulates ECT-2 asymmetry by promoting an enrichment of ECT-2 at the anterior cortex in phase I (Fig. 5). Further evidence for the involvement of CDC-42 in efficient polarization is that the rate of cortical actomyosin flow during phase I is significantly reduced in *cdc-42 (RNAi)* embryos (maximum speeds in wild-type = 7.8 ± 1.1 μm min^{-1} versus those in *cdc-42 (RNAi)* embryos = 3.4 ± 1.5 μm min^{-1}; see Supplementary Information, Fig. S2c, d). These results indicate that CDC-42 is involved in a positive feedback mechanism that facilitates the initial polarization process.

Local relaxation of the global contractility of the cortex is thought to drive cortical flow away from the centrosome[22]. Our results provide a basis for understanding how the polarity cue from the centrosome

releases the contractility of the cortical actomyosin cytoskeleton in a local posterior region (Fig. 5). The SPD-5-dependent cue from the centrosome induces the exclusion of ECT-2 from the cortex nearest to the centrosome, which then causes a local depletion of cortical RHO-1 at the posterior cortex. The resulting RHO-1 depletion would cause a local decrease in the myosin-dependent contractions of the cortical actomyosin network or of actomyosin renewal through a continuous assembly/disassembly cycle, which would lead to a local break in the actomyosin network that homogeneously covers the entire cortex. This gradient in actomyosin-mediated tension should drive the cortical flows away from the centrosome, which would result in the asymmetric distribution of the anterior PAR complex and CDC-42 at the anterior cortical domain (Fig. 5; phase I). Our results also suggest that polarized CDC-42 may modulate ECT-2 asymmetry (Fig. 5; phase I, dotted line), although its mode of action is unknown. This positive feedback mechanism may function to reinforce the initial anterior–posterior polarization.

After the initial polarization by the cortical actomyosin flow, anteriorly enriched CDC-42 mediates a reorganization of the actomyosin network at the anterior cortex to maintain the anterior cortical domain of PAR proteins (Fig. 5; phase II). It was previously proposed that polarization occurs in two phases: an 'establishment' phase before pronuclear meeting; and a 'maintenance' phase after pronuclear meeting[9]. In the maintenance phase, which temporally overlaps with phase II in our study, the posteriorly localized PAR-2 keeps anterior PAR proteins out of the posterior cortex by inhibiting recruitment of cortical myosin to the posterior cortical domain[1,9]. Therefore, CDC-42 and PAR-2 concomitantly contribute to maintaining the anterior and posterior cortical domains, respectively. Although Cdc42 is known to regulate the actin cytoskeleton through multiple effectors in other organisms[23], how CDC-42 affects the cortical actomyosin organization in *C. elegans* has yet to be determined.

In summary, our data place cortical ECT-2 at the top of the hierarchy in the small G-protein cascade that regulates the formation of cortical polarity in early *C. elegans* embryos. ECT-2 may be the primary target of the centrosomal polarity cue. We have also shown that the sequential functions of two Rho family GTPases, RHO-1 and CDC-42, are crucial for the establishment of anterior–posterior polarity in the *C. elegans* embryo. In many types of cells in various organisms, Cdc42 and the Par3–Par6–aPKC complex are implicated in the establishment of cell polarity[23]. In mammals, the quaternary Cdc42–Par3–Par6–aPKC complex is formed *in vivo*, in at least some physiological contexts[24], but how the polarity cues relocate Cdc42 to the restricted site has been unclear. Our investigations using *C. elegans* embryos show that the break in the symmetry of the actomyosin network that is triggered by the local exclusion of ECT-2 and RHO-1 is the prerequisite for the PAR complex- and CDC-42-dependent process of polarity establishment. Thus, it will be of interest to investigate whether this hierarchical functioning of these Rho GTPases represents a conserved framework for the polarization process in other organisms. □

METHODS

GFP fusions. The following integrated transgenic lines were used: GFP–PAR-6, *axIs1137[pRF4 + pJH7.04 + par-6::gfp]*[9]; GFP–RHO-1, *tjIs1*[*unc-119(+) pie-1 promoter::gfp::rho-1*][15]; GFP–moe, *nnIs1*[*unc-119(+) pie-1 promoter::gfp::moesin*][15]; GFP–$PH^{PLC1\delta1}$, *ltIs38*[*unc-119(+) pie-1 promoter::gfp::*$PH^{PLC1\delta1}$][18]; GFP–ECT-2, *tjIs4*[*unc-119(+) pie-1 promoter::gfp::ect-2*]; GFP–CDC-42, *tjIs6*[*unc-119(+) pie-1 promoter::gfp::cdc-42*] and GFP–PLK-1, *tjIs5*[*unc-119(+) pie-1 promoter::gfp:plk-1*]. To generate these strains, PCR-amplified cDNA fragments of *ect-2*, or PCR-amplified genomic fragments of *cdc-42* and *plk-1*, were inserted into pID3.01B (gift from G. Seydoux, Johns Hopkins University School of Medicine, Baltimore, MD) using Gateway Technology (Invitrogen, Carlsbad, CA) as per the manufacturers' instructions. Ballistic transformation was carried out as previously described[25].

RNA interference. RNAi was carried out by the soaking method[26,27]. cDNA clones (gift from Y. Kohara, National Institute of Genetics, Mishima, Japan) were as follows: yk651f5 (*rho-1*), yk325h8 (*spd-5*), yk396b7 (*par-3*), yk64a7 (*par-2*) and yk116c12 (*ect-2*). dsRNA of *cdc-42*, *pfn-1* and *mlc-4* was prepared from the appropriate cDNA cloned into the vector pDONR201. Worms were soaked in dsRNA solution at concentrations between 1 and 5 mg ml^{-1} and were incubated at 20 °C for 24 h. The worms were then cultured at 20 °C and observed for 20–28 h after removal from the dsRNA solution.

Live imaging and analysis of GFP fluorescence. Gravid worms in egg salt buffer[28] were dissected on coverslips, which were then inverted onto 2% agarose pads and sealed with Vaseline. Embryos were observed at 20 °C with an UplanApo 100× 1.35 NA oil immersion lens using a CSU21 spinning-disc confocal system (Yokogawa Electric Corp., Tokyo, Japan) mounted on a BX51 upright microscope (Olympus, Tokyo, Japan). The specimens were illuminated with a Sapphire488 semiconductor laser (Coherent Laser Division, Santa Clare, CA). Images were acquired with an Orca ER 12-bit cooled CCD camera (Hamamatsu Photonics, Shizuoka, Japan) and the acquisition system was controlled by IP Lab software (Scanalytics, Inc., Fairfax, VA). For quantitative analysis of the fluorescence images, images were acquired every 10 s using a 400–500 ms exposure at 100% power on the 20 mW laser and 2 × 2 binning in the camera. Under these conditions, pixels were not saturated. Additional image processing was done with Adobe Photoshop (Adobe Systems, San Jose, CA).

For kymograph analysis, cortical regions of interest (the equatorial region along the long axis of the cell) were cropped and stacked horizontally into kymograph images using IP Lab software. The resulting image was a two-dimensional representation of the time-lapse movie, with the *y* axis corresponding to time. All signals of the GFP fusions in the cropped regions appeared as dots or lines.

To analyse the distribution of cortical GFP–PAR-6 or GFP–moe signals, the cortical regions were divided into anterior and posterior halves and the total intensity of the GFP fluorescence in these regions was measured using Metamorph software (Universal Imaging Corp., Sunnyvale, CA). The average intensity of seven wild-type embryos (without the GFP transgene) were subtracted as a background signal; more than seven embryos were analysed for each genotype.

For the line-scan analysis of cortical GFP–ECT-2, the fluorescence intensity along the cortex (1 pixel width) was determined using Metamorph software. The region of the cortex that was depleted of GFP–ECT-2 fluorescence was defined as showing less than half of the averaged fluorescence intensity in the dorsal or ventral cortical region.

The distribution of the cortical GFP–RHO-1 and GFP–CDC-42 foci was analysed as follows: the fluorescent signals other than the cortical foci were removed from each image using a common threshold value determined from the GFP–RHO-1 or GFP–CDC-42 images of wild-type embryos; areas of the anterior and posterior cortical regions and those covered by GFP foci (that is, the areas above the threshold value) in each region were measured using the Integrated Morphometry Analysis function in Metamorph software, and the percentage of the area that was covered by the foci was calculated for more than six embryos for each genotype.

Note: Supplementary Information is available on the Nature Cell Biology website.

ACKNOWLEDGMENTS

We thank N.V. Velarde and F. Piano for kindly providing the strain expressing GFP–moe and for sharing information before publication; F. Matsuzaki for suggestions and thoughtful comments on the manuscript; and G. Seydoux, D. Kiehart, K. Kemphues, A. Audhya and Y. Kohara for their generous gifts of reagents. We also thank Y. Kodama for the initial characterization of the *ect-2* gene and all members of our laboratories for helpful discussions. Some of the worm strains used in this study were provided by the *Caenorhabditis* Genetics Center, which is funded by the National Institutes of Health (NIH) National Center for Research Resources. This work was supported by a Grant-in-Aid for Scientific Research on Priority Areas 'Systems Genomics' (A.S.) and a Grant-in-Aid for Young Scientists B (F.M.) from

the Ministry of Education, Culture, Sports, Science and Technology of Japan. F.M. was supported by the Special Postdoctoral Researchers Program of RIKEN.

AUTHOR CONTRIBUTIONS

F.M. designed and performed the experiments. F.M. and A.S. performed the data analysis and wrote the paper. A.S. was responsible for project planning and guidance.

COMPETING FINANCIAL INTERESTS

The authors declare that they have no competing financial interests.

Published online at http://www.nature.com/naturecellbiology/
Reprints and permissions information is available online at http://npg.nature.com/reprintsandpermissions/

1. Munro, E., Nance, J. & Priess, J. R. Cortical flows powered by asymmetrical contraction transport PAR proteins to establish and maintain anterior-posterior polarity in the early *C. elegans* embryo. *Dev. Cell* **7,** 413–424 (2004).
2. Morita, K., Hirono, K. & Han, M. The *Caenorhabditis elegans ect-2* RhoGEF gene regulates cytokinesis and migration of epidermal P cells. *EMBO Rep.* **6,** 1163–1168 (2005).
3. Kemphues, K. PARsing embryonic polarity. *Cell* **12,** 345–348 (2000).
4. Gotta, M., Abraham, M. C. & Ahringer, J. CDC-42 controls early cell polarity and spindle orientation in *C. elegans*. *Curr. Biol.* **11,** 482–488 (2001).
5. Kay, A. J. & Hunter, C. P. CDC-42 regulates PAR protein localization and function to control cellular and embryonic polarity in *C. elegans*. *Curr. Biol.* **11,** 474–481 (2001).
6. Cowan, C. R. & Hyman, A. A. Asymmetric cell division in *C. elegans*: cortical polarity and spindle positioning. *Annu. Rev. Cell Dev. Biol.* **20,** 427–453 (2004).
7. Cowan, C. R. & Hyman, A. A. Centrosomes direct cell polarity independently of microtubule assembly in *C. elegans* embryos. *Nature* **431,** 92–96 (2004).
8. Wallenfang, M. R. & Seydoux, G. Polarization of the anterior-posterior axis of *C. elegans* is a microtubule-directed process. *Nature* **408,** 89–92 (2000).
9. Cuenca, A. A., Schetter, A., Aceto, D., Kemphues, K. J. & Seydoux, G. Polarization of the *C. elegans* zygote proceeds via distinct establishment and maintenance phases. *Development* **130,** 1255–1265 (2003).
10. Guo, S. & Kemphues, K. J. A non-muscle myosin required for embryonic polarity in *Caenorhabditis elegans*. *Nature* **382,** 455–458 (1996).
11. Hill, D. P. & Strome, S. An analysis of the role of microfilaments in the establishment and maintenance of asymmetry in *Caenorhabditis elegans* zygotes. *Dev. Biol.* **125,** 75–84 (1988).
12. Shelton, C. A., Carter, J. C., Ellis, G. C. & Bowerman, B. The nonmuscle myosin regulatory light chain gene *mlc-4* is required for cytokinesis, anterior-posterior polarity, and body morphology during *Caenorhabditis elegans* embryogenesis. *J. Cell Biol.* **146,** 439–451 (1999).
13. Severson, A. F. & Bowerman, B. Myosin and the PAR proteins polarize microfilament-dependent forces that shape and position mitotic spindles in *Caenorhabditis elegans*. *J. Cell Biol.* **161,** 21–26 (2003).
14. Hall, A. Rho GTPases and the actin cytoskeleton. *Science* **279,** 509–514 (1998).
15. Motegi, F., Velarde, N. V., Piano, F. & Sugimoto, A. Two phases of astral microtubule activity during cytokinesis in *C. elegans* embryos. *Dev. Cell* **10,** 509–520 (2006).
16. Jantsch-Plunger, V. *et al.* CYK-4: A Rho family GTPase activating protein (GAP) required for central spindle formation and cytokinesis. *J. Cell Biol.* **149,** 1391–1404 (2000).
17. Dechant, R. & Glotzer, M. Centrosome separation and central spindle assembly act in redundant pathways that regulate microtubule density and trigger cleavage furrow formation. *Dev. Cell* **4,** 333–344 (2003).
18. Audhya, A. *et al.* A complex containing the Sm protein CAR-1 and the RNA helicase CGH-1 is required for embryonic cytokinesis in *Caenorhabditis elegans*. *J. Cell Biol.* **171,** 267–279 (2005).
19 Hamill, D. R., Severson, A. F., Carter, J. C. & Bowerman, B. Centrosome maturation and mitotic spindle assembly in *C. elegans* require SPD-5, a protein with multiple coiled-coil domains. *Dev. Cell* **3,** 673–684 (2002).
20. Nishimura, Y. & Yonemura, S. Centralspindlin regulates ECT2 and RhoA accumulation at the equatorial cortex during cytokinesis. *J. Cell Sci.* **119,** 104–114 (2006).
21. Yuce, O., Piekny, A. & Glotzer, M. An ECT2-centralspindlin complex regulates the localization and function of RhoA. *J. Cell Biol.* **170,** 571–582 (2005).
22. Hird, S. N. & White, J. G. Cortical and cytoplasmic flow polarity in early embryonic cells of *Caenorhabditis elegans*. *J. Cell Biol.* **121,** 1343–1355 (1993).
23. Etienne-Manneville, S. Cdc42 — the centre of polarity. *J. Cell Sci.* **117,** 1291–1300 (2004).
24. Joberty, G., Petersen, C., Gao, L. & Macara, I. G. The cell-polarity protein Par6 links Par3 and atypical protein kinase C to Cdc42. *Nature Cell Biol.* **2,** 531–539 (2000).
25. Praitis, V., Casey, E., Collar, D. & Austin, J. Creation of low-copy integrated transgenic lines in *Caenorhabditis elegans*. *Genetics* **157,** 1217–1226 (2001).
26. Maeda, I., Kohara, Y., Yamamoto, M. & Sugimoto, A. Large-scale analysis of gene function in *Caenorhabditis elegans* by high-throughput RNAi. *Curr. Biol.* **11,** 171–176 (2001).
27. Sumiyoshi, E., Sugimoto, A. & Yamamoto, M. Protein phosphatase 4 is required for centrosome maturation in mitosis and sperm meiosis in *C. elegans*. *J. Cell Sci.* **115,** 1403–1410 (2002).
28. Edger, L. G. Blastmere culture and analysis. *Methods Cell Biol.* **48,** 303–321 (1995).

nature cell biology

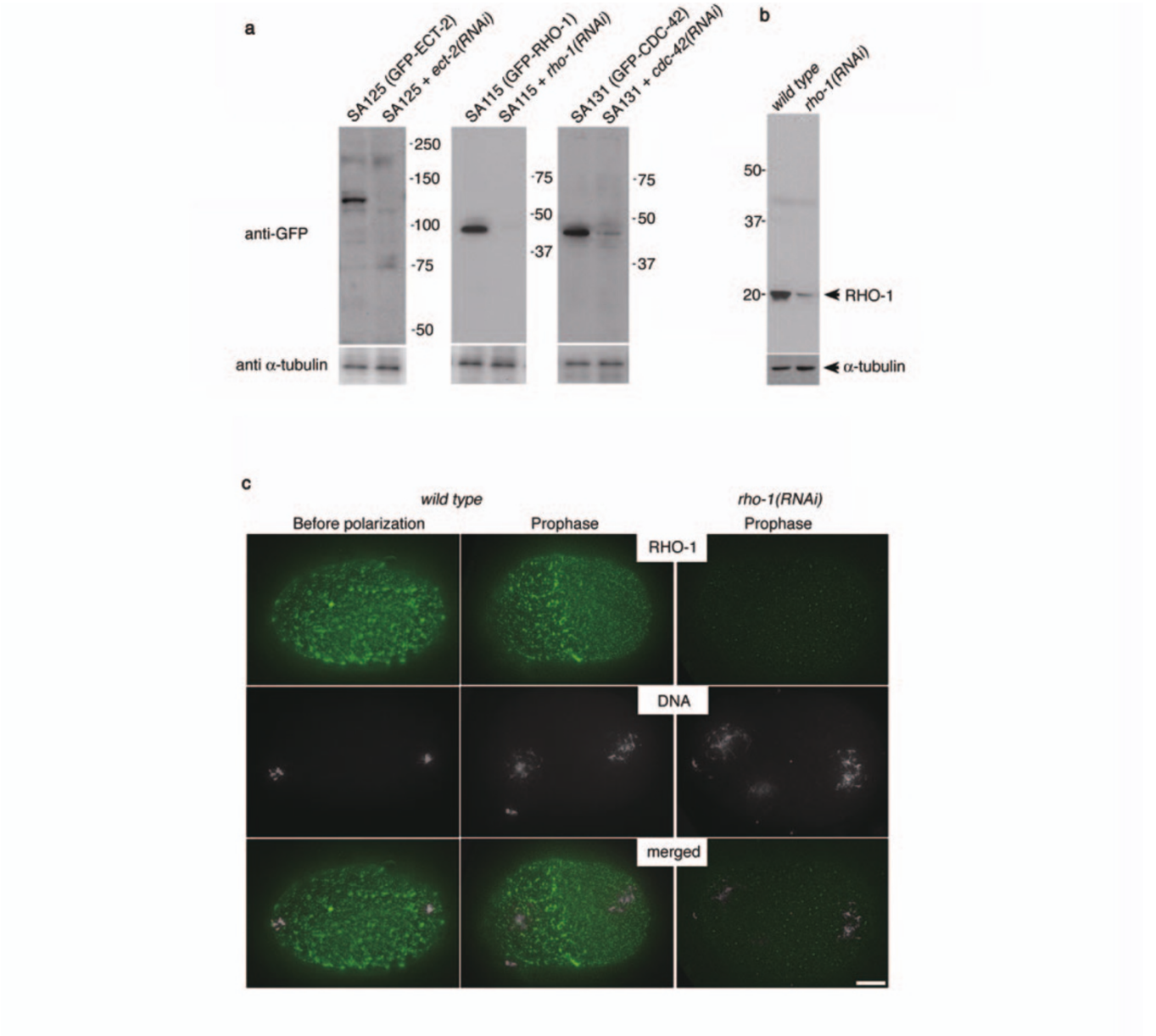

Figure S1 Evaluation of protein depletion by RNAi. (a) Immunoblot analysis of strains expressing GFP-ECT-2 (SA125; left), GFP-RHO-1 (SA115; middle) or GFP-CDC-42 (SA131; right) using antibodies against GFP. Extracts from wild-type worms (left lanes) and those from RNAi-treated worms (right lanes) are shown. Detected bands correspond to the expected size of the GFP fusion proteins. α-tubulin was used as a loading control. (**b**) Immunoblot analysis using antibodies against RHO-1. Anti-RHO-1 detected a single band of ~20 kDa in extracts prepared from wild-type adult worms (left). Comparison with the *rho-1(RNAi)* worm extract indicates that 88% of RHO-1 was depleted by RNAi. α-tubulin was used as a loading control. **(c)** Immunofluorescence using RHO-1 antibodies. Wild-type (left and middle) and *rho-1(RNAi)* (right) embryos before polarization (left) and at mitotic prophase (middle and right) were stained with anti-RHO-1 (green) and DAPI (white). Developmental stages were defined based on chromosome morphology. RHO-1 was found throughout the cortex before polarization but was more concentrated in the anterior cortical region than the posterior cortical region at mitotic prophase. Bar, 10 μm.

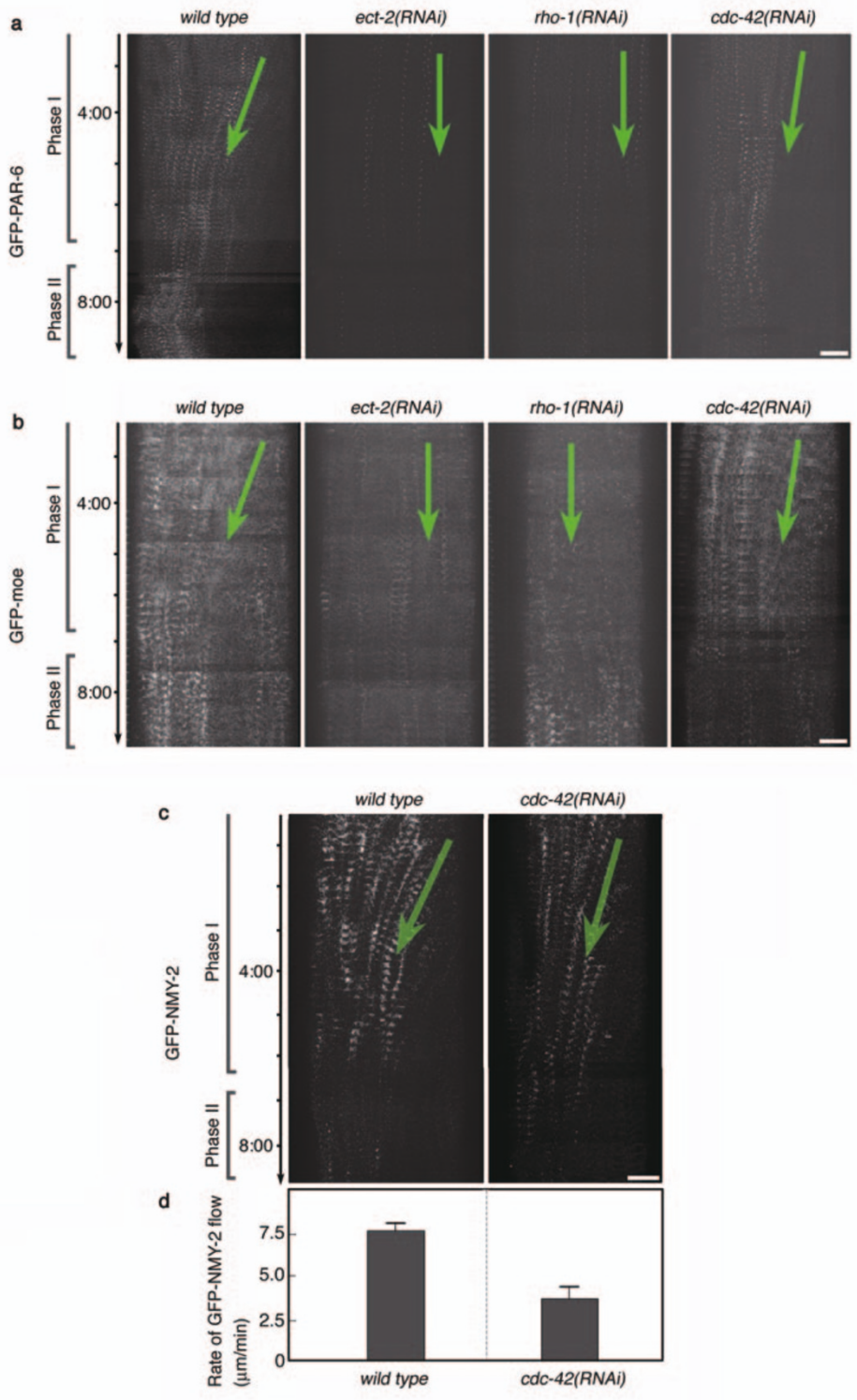

Figure S2 Kymograph analysis of GFP-PAR-6, GFP-moe, and GFP-NMY-2 behavior during the polarization process. (**a-c**) Representative kymographs of GFP-PAR-6 (**a**), GFP-moe (**b**) and GFP-NMY-2 (myosin heavy chain)[2] (**c**) at the cortex during the polarization process. Regions of equatorial cortex along the long axis were cropped and stacked horizontally into kymograph images. Green arrows mark a selected trajectory of the GFP signals. Times are with respect to the appearance of sperm pronuclei, as judged by DIC observation (min:s). Bar, 10 μm. (**d**) Comparison of the maximum speed of the GFP-NMY-2 flow in wild-type and *cdc-42(RNAi)* embryos. The flow of GFP-NMY-2 toward the anterior cortex showed a statistically significant difference between wild-type embryos and *cdc-42(RNAi)* embryos (*t*-test, $P < 0.05$). The data are the mean (s.d. of >12 foci from 4 independent embryos.

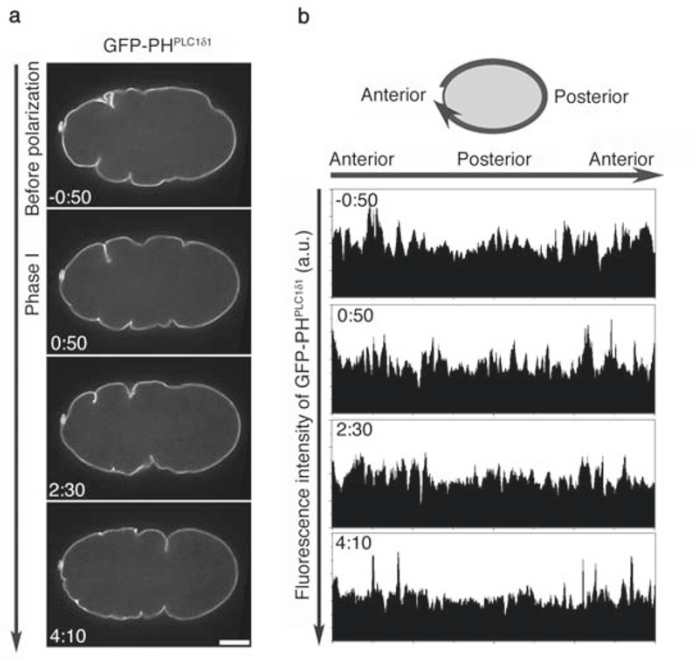

Figure S3 A plasma membrane marker GFP-PH$^{PLC1\delta1}$ was not locally excluded during A-P polarity establishment. (**a**) Time-lapse images of GFP-PH$^{PLC1\delta1}$ at the medial focal plane during polarization. Times are with respect to the onset of posterior cortical smoothing (min:s). Bar, 10 μm. (**b**) Line scan analysis of fluorescence intensities of cortical GFP-PH$^{PLC1\delta1}$ during polarization. Top diagram: A curved line from anterior pole to anterior pole marks the cortical region from which the line scan was made. This curve was linearized to make the line scan. Unlike GFP-ECT-2, GFP-PH$^{PLC1\delta1}$ fluorescence was not decreased at the posterior-most cortex during the establishment of A-P polarization.

Supplementary Movie 1 GFP-ECT-2 dynamics during the establishment of A-P polarity.
Dynamics of GFP-ECT-2 at the medial focal plane are shown. Images were acquired with a 0.5-s exposure time at 10-s intervals.

Supplementary Movie 2 GFP-RHO-1 dynamics during the establishment of A-P polarity.
Dynamics of GFP-RHO-1 at the cortical focal plane are shown. Images were acquired with a 0.5-s exposure time at 5-s intervals.

Supplementary Movie 3 GFP-CDC-42 dynamics during the establishment of A-P polarity.
Dynamics of GFP-CDC-42 at the cortical focal plane are shown. Images were acquired with a 0.5-s exposure time at 10-s intervals.

REFERRENCES

1. Yonemura, S., Hirao-Minakuchi, K., & Nishimura, Y. Rho localization in cells and tissues. *Exp. Cell Res.* **295**, 300-314 (2004).
2. Nance, J., Munro, E. & Priess, J. R. *C. elegans* PAR-3 and PAR-6 are required for apicobasal asymmetries associated with cell adhesion and gastrulation. *Development* **130**, 5339-5350 (2003).

Fumio Motegi & Asako Sugimoto

"Sequential functioning of ECT-2/RhoGEF, RHO-1 and CDC-42 establishes cell polarity in *C. elegans* embryos"

Supplementary Information

METHODS

Antibodies and immunostaining. RHO-1 antibodies (anti-RHO-1) were prepared using His-tagged RHO-1 fusion protein to immunize two rabbits, and RHO-1-specific antibodies were then affinity purified using an immobilized GST-tagged RHO-1 fusion protein. Indirect immunostaining for RHO-1 was carried out using a modified version of a published protocol[1]: embryos were fixed in 10% trichloroacetic acid solution at 4 ºC for 40 min, washed with PBS and incubated with a 1:200 dilution of affinity-purified anti-RHO-1. The secondary antibodies used were a 1:1,000 dilution of Alexa-488-conjugated goat anti–rabbit IgG (Molecular Probes). Slides were counterstained with 2 mg/ml DAPI. Images were acquired with an UplanApo 100× 1.35 NA oil immersion lens using a wide-field Delta Vision microscope (Applied Precision) with an IX70 inverted microscope (Olympus). Images were processed in Adobe Photoshop.

Immunoblotting. For immunoblotting experiments, 50-µl volumes of worms were washed three times with M9. An equal volume of lysis buffer (50 mM HEPES, pH 7.4; 1 mM EGTA; 1 mM $MgCl_2$; 100 mM KCl; 10% (w/v) glycerol) and two volumes of glass beads were added, and the tubes were agitated vigorously. An equal volume of 2× sodium dodecyl sulfate–polyacrylamide gel electrophoresis (SDS-PAGE) sample buffer was added and boiled for 5 min. SDS-PAGE and western blot analysis were carried out according to standard procedures. Primary antibodies against GFP (sc8334; Invitrogen) or α-tubulin (DM1A; Sigma) were used at 1:3,000, and those against RHO-1 were used at 1:10,000. The HRP-conjugated goat anti-mouse or anti-rabbit secondary antibodies (Amersham) were used at 1:8,000, and the signal was detected with standard chemiluminescence (Amersham).